Article

Not peer-reviewed version

# Steel Sheet Deformation in Clinch-Riveting Joining Process

Waldemar Witkowski *, Jacek Mucha, Łukasz Boda

Posted Date: 22 February 2024

doi: 10.20944/preprints202402.1272.v1

Keywords: sheet deformation clinch-rivet joint; GOM measurements; DX51+Z275 steel sheet

 doi:10.20944/preprints202402.1272.v1



*Article*

# Steel Sheet Deformation in Clinch-Riveting Joining Process

**Waldemar Witkowski [1,*], Jacek Mucha [1] and Łukasz Boda [2]**

[1] Faculty of Mechanical Engineering and Aeronautics, Rzeszow University of Technology, Al. Powstancow Warszawy 8, 35-959 Rzeszow, Poland; wwitkowski@prz.edu.pl; j_mucha@prz.edu.pl
[2] Doctoral School of the Rzeszow University at Technology, Al. Powstancow Warszawy 12, 35-959 Rzeszow, Poland; d413@stud.prz.edu.pl
* Correspondence: wwitkowski@prz.edu.pl; Tel.: +48-178652397

**Abstract:** This paper presents the deformation of the joined sheet after the clinch-riveting process. The DX51D steel sheet with zinc coating was used. The samples to be joined with clinch riveting technology had a thickness of 1±0.05 mm and 1.5±0.1 mm. The sheet deformation was measured before and after the joining process. The rivet was pressed in the sheets with the same dimension between the rivet axis and three sheet edges: 20, 30 and 40 mm. For fixed segments of the die, from the rivet side close to the rivet, the sheet deformation was greater than that of the area with movable segments. The movement of die sliding element caused more sheet material to flow in the space between the fixed part of the die and movable segments. Hence, the sheet deformation in these places was smaller than for the die fixed element – sheet material was less compressed. For sheets thickness 1.5 mm and width 20 mm, the bulk of the sheet was observed. For a sheets width of 20 mm, it was observed that the deformation of the upper and lower sheets in the area of the rivet is greater than for sheets width of 30 or 40 mm.

**Keywords:** sheet deformation clinch-rivet joint; GOM measurements; DX51+Z275 steel sheet

## 1. Introduction

Manufacturing elements with a specific geometric quality is still a challenge. Despite the improvement in the design of machines and machine tools, plastically formed elements sometimes show unpredictable shape changes during the manufacturing or joining process. The technological parameters of the plastic forming processes influence the deformations and dimensional accuracy of the manufactured elements. Cold- and hot-formed thin-walled metal and plastic elements require different control techniques [1,2]. Geometric variability occurs when the thermal energy necessary to form the joint is supplied locally [3]. As a result of progress, including the introduction of new assembly technologies, there is a need to develop control and assessment of the shape and dimension quality of products. In addition to the technological parameters of the assembly process, the location of the joint in the thin-walled structure is very important. Designers of thin-walled structures often have limitations on the location of joints. The shorter the distance from the edge of the sheet, the smaller the width of the material band needed to form the joint. Less material means less additional weight in the thin-walled structure. The close location of the joint to the edges of the connected layers (or one of them) causes large deformations (Figure 1).

 doi:10.20944/preprints202402.1272.v1



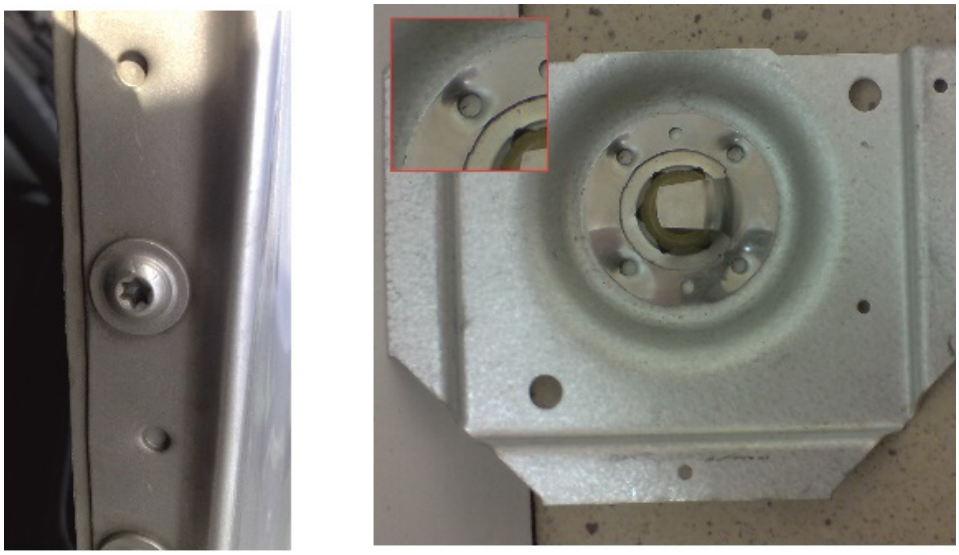

(a) (b)

**Figure 1.** Example of the clinch joint formed close to the sheets edge: a) aluminium alloy sheets, b) thin stainless steel sheet and thick carbon steel sheet.

During the assembly processes of thin-walled elements, there is a varying intensity of interference in the material structure of the joined elements. Each thin-walled element processing and assembly technology causes shape deformations and changes in the dimensions of the designed element [4,5]. Deformations resulting from springing in the joint area are also very important [6,7]. As a result of joining the sheets, local action on the material may cause them to spread apart (Figure 2). When joining thin-walled elements, it is important that such deformations are very small. Their complete elimination is difficult and requires a series of tests to determine the parameters of the joining process.

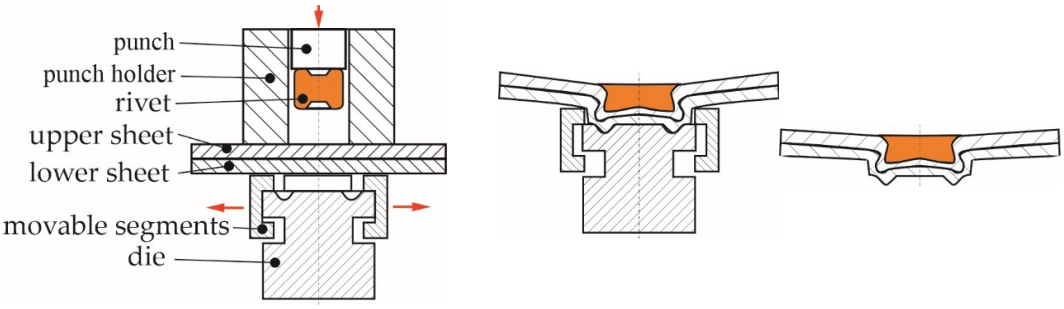


**Figure 2.** The characteristic of sheet deformation in clinch riveting process: a) before joining, b) after punch retract, c) after die retract.

Automotive manufacturers are increasingly using pressed-joining technologies. This group of connecting technologies includes, among others: self-piercing riveting (“SPR”) [8–11], clinching (“CL”) [12–17], solid self-piercing riveting (“SSPR”) [18–24] and clinch-riveting (“CR”) [25–31]. Companies see more and more potential for this group of pressed joints. It is often necessary to connect more than two layers of material, this is possible due to technology, for example, “SPR” [32–34]. In the case of clinching joints, it is also possible to make a three-layer joint for certain material arrangements [35]. Each joining technique has its limitations and dedicated applications. The type of materials, their thickness, the arrangement of tools and material layers, and the amount of forming force are very important. When pressed joints are formed, including clinching, especially in the case

 doi:10.20944/preprints202402.1272.v1



of high-strength materials, significant tool loads occur [36]. The use of the above-mentioned joining methods in the case of metallic materials does not require drilling a hole before joining. It is possible to combine composites with metallic materials, with certain limitations. When composite is the upper layer and metal is the lower layer, for some arrangements "SPR" joint [37–40], clinching [41–45] or solid self-piercing riveting [41,46] can be formed. There are an increasing number of industrial applications that involve the joining of composite elements using the above mentioned pressure joining techniques [43,47]. Joining of composite and metal using a punching rivet and heating to 180°C was presented, for example, in [48]. If the lower layer is less plastic and the upper layer is more plastic, it is possible to connect them by clinching, when a hole is made in the lower layer for two sheets [49] or even three sheets [50]. The reverse combination of the material arrangement, i.e., the upper one is composite and the lower one is metal, when a hole is made, is possible to create a joint. However, composite fibres are subject to significant deformation [51]. If the lower layer is a composite and the upper layer is a metal, it is possible to join them by clinching, but this requires heating of the joined materials [52]. However, heating the material causes additional subsequent return deformations, which affect the deformation of the shape and dimensions of the joined elements.

This publication presents the influence of using different values of the width of the joined sheet samples and the distance of the joint axis from the external edges of the sheets on the amount of deformation of the joined elements. The joints were made using clinch-riveting technology. The tests were carried out to join two sheets of thicknesses of 1.0 mm and 1.5 mm made of DX51D steel. The joints were experimentally formed and the influence of the distance of the joint in the lap joint on the forming force and the amount of deformation of the joined elements near the joint was analysed.

## 2. Experimental measurements

### *2.1. Sheet material*

Steel sheets are commonly used in light gauge profiles and thin-walled structures. Experimental tests of the sheet deformation were conducted for the DX51D steel sheet (material number 1.0226, according to the EN 10327:2004 standard [53]) with ZiNc coating. The samples for joining by clinch riveting technology had a thickness of 1±0.05 mm and 1.5±0.1 mm. Grammage of the zinc layer was 275 g/m$^2$ with thickness about 20 µm. Basic mechanical properties were presented in Table 1 (average values), and the chemical composition were shown in Table 2 (maximum content).

**Table 1.** Mechanical properties of DX51D+Z275 sheets.

| Material Designation | Surface Finish + Z, [g/m$^2$] | Young's Modulus $E$, [GPa] | Poisson's Ratio $\nu$, [-] | Yield Strength $R_{p0.2}$, [MPa] | Tensile Strength $R_m$, [MPa] | Elongation after Fracture $A_{80}$,[%] |
|---|---|---|---|---|---|---|
| DX51D+Z275 | zinc layer quality 275 | 188 | 0.3 | 330 | 438 | 29 |

**Table 2.** Chemical composition of DX51D+Z275 sheets (maximum percentage by weight [%]).

| Mn | Si | Ti | C | P | S | Fe |
|---|---|---|---|---|---|---|
| 1.2 | 0.5 | 0.3 | 0.18 | 0.12 | 0.045 | remainder |

### *2.2. Clinch-riveting joining process*

Clinch riveted joints were performed in the Pressed Joint Laboratory of the Machine Design Department at Rzeszow University of Technology (Rzeszow, Poland). The TOX Pressotechnik machine (Figure 3) was used to prepare joint samples. Maximum joining force generated by EMPK electric drive system (Tox Pressotechnik, Wroclaw, Poland) is 100 kN. The die is fixed to the C-frame body. The punch system, driven by EMPK system, is moved in vertical axis. The accuracy of the punch system displacement is 0.01 mm. The strain gauge system is measuring the forming force with the accuracy up to 0.5%.

 doi:10.20944/preprints202402.1272.v1



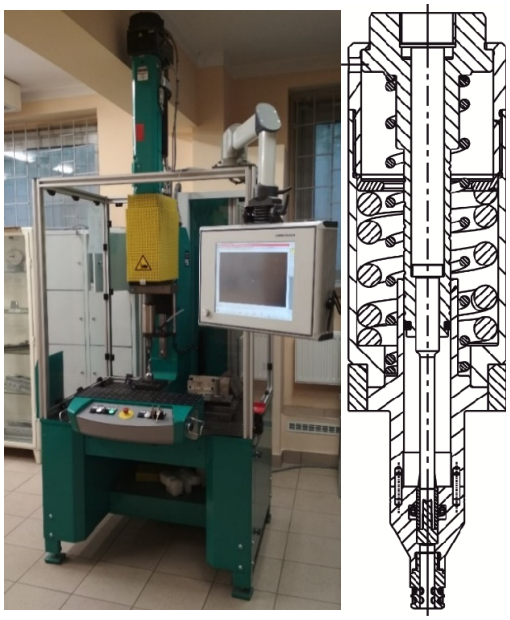


**Figure 3.** The C-frame stand for forming CR joints: a) C-frame machine, b) cross section of the punch system with rivet feeder.

For preparing clinch riveted joints the "SKB" die, with movable segments were used, and punch system, with rivet feeder, and "TOX Pressotechnik" steel rivets were used. The die has a four fixed parts and four movable segments. The geometry and main dimension of the die were presented in Figure 4a. The punch system consists of punch, blank holder with spring and rivet feeder system. The geometry and main dimension of the punch and blank holder were presented in Figure 4b. The deformable steel rivets (type A5x5-2Al), manufactured by "TOX Pressotechnik", had a hardness of 400HV1 (average values from 5 measurements). Hardness measurement, using the Vickers method, was performed using a Matsuzawa microhardness tester (type Micro-Sa, Seiki Co., Ltd.) (Nagaoka-shi, Japan). The measurement load was 10 N (in accordance with the ISO 6507-1:2018 standard [54]). The characteristics of the rivets have been presented in other papers [27,30].

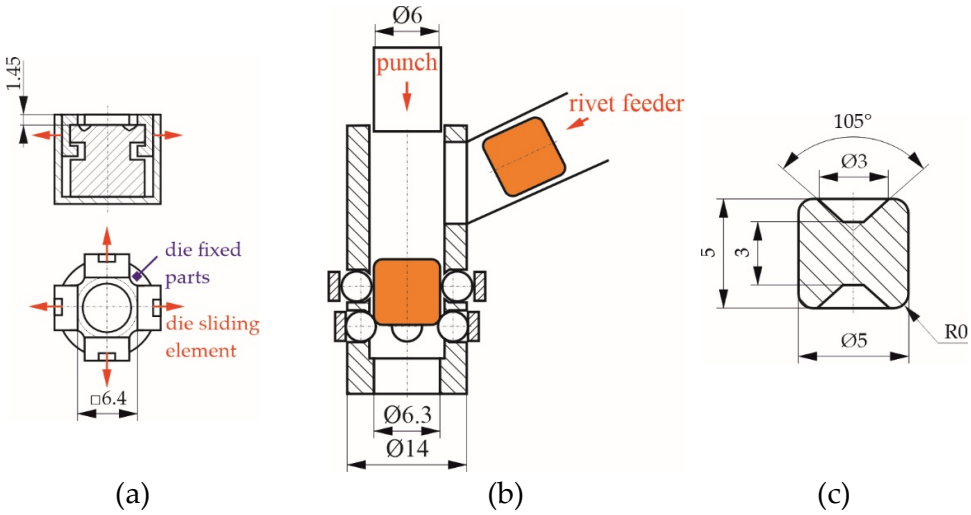


**Figure 4.** The basic forming tools used in clinch riveting technology: a) die, b) punch system, c) rivet.

The geometry and dimensions of used rivets were presented in Figure 4c. The example of the forming force-displacement diagram from clinch riveting process was presented in Figure 5. The

 doi:10.20944/preprints202402.1272.v1



maximum punch movement along vertical axis was set up to obtain the same level of the top surface of the rivet and the top surface of upper sheet.

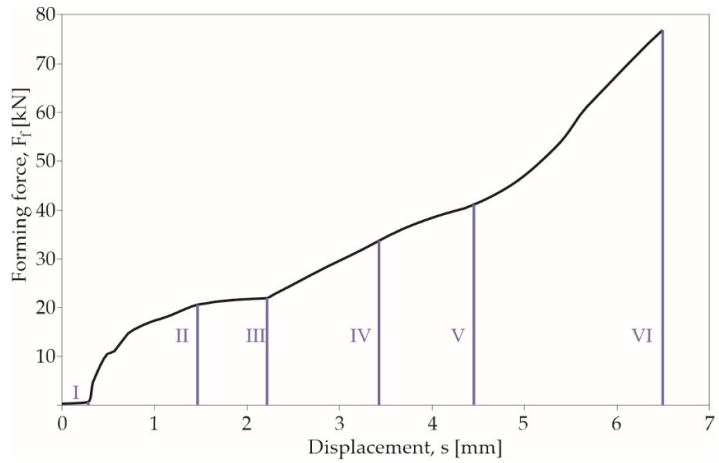


**Figure 5.** The force-displacement diagram of clinch riveting process.

In the clinch riveting process seven phases can be observed:

- phase I - special rivet feeder with an automatic rivet insertion mechanism positioned the rivet by the movement of the holder springs (at two levels),
- phase II - rivet contacted the upper sheet,
- phase III - rivet was pressed with sheets into the die groove,
- phase IV - the lower surface of the lower sheet touch with the bottom surface of the die,
- phase V - the rivet material filled the free space formed after the movement of the sheet material in the die cavity and space formed after displacement of the die movable segments,
- phase VI - the rivet material was flow intensively in its lower part in the transverse direction – the joint interlock was formed,
- phase VII - the punch system move to basic point.

In Figure 5 only phases from 2 to 6 were presented. The phase 1 and 7 are not closely related to the formation of the joint – they are a preparatory-completion movements. So the force and displacement values at this movements were not recorder.

*2.3. Sheet deformation measurements*

All samples were cut out form sheets with dimension 2500x1250x1.0 mm and 2500x1250x1.5 mm. The sheet samples deformation was measured before (Figure 6a) and after (Figure 6b) joining process. The rivet was pressed in the sheet with ensuring the same dimension (b) between rivet axis and three sheet edges (sheet width divided by two) – Figure 7. The measurements of the sheet deformation were made for two sheet thickness (1 and 1.5 mm) of clinch-rivet joints and for three values of the sheet width ($b$=20, 30 and 40 mm). In Figure 7 the scheme of the measurement point coordinates for chosen angles (0°, 45°, 90°, 180° and 270°) was presented.

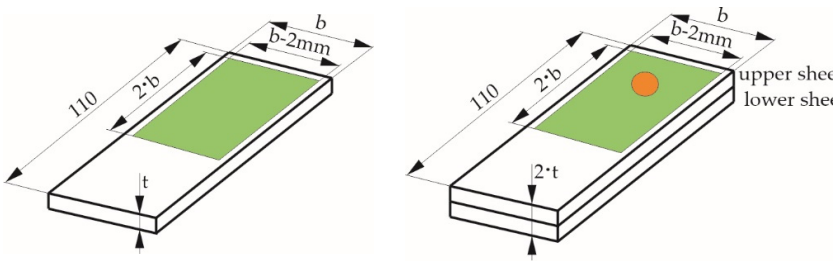

 doi:10.20944/preprints202402.1272.v1



**Figure 6.** The samples and measuring areas dimensions: a) before joining, b) after joining.

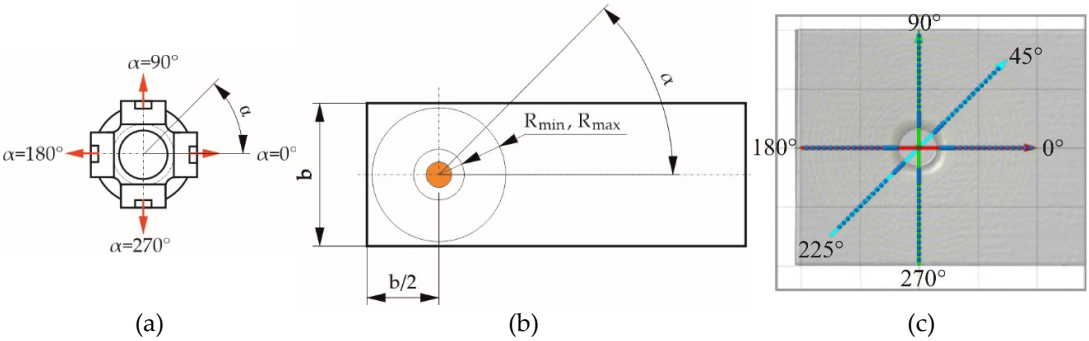


**Figure 7.** The scheme of the measurements: a) position of the movable segments of the die, b) radius dimension c) angles for joint cross-sections.

The measurement radius was changed from $R_{min}$ to $R_{max}$. The radius of measurement points was chosen from $R_{min}$=3.75 mm to dimension equal $R_{max}$=$b$-2 mm depending on the sheet width. The minimum and maximum dimension of the measurement radius for alle sheet width are presented in Table 3.

**Table 3.** The dimensions of the measurement radius.

| Sheet width $b$, [mm] | Sheet thickness $t$, [mm] | $R_{min}$, [mm] | $R_{max}$, [mm] |
|---|---|---|---|
| 20 | 1 | 3.75 | 9 |
| 30 | 1 | 3.75 | 14 |
| 40 | 1 | 3.75 | 19 |
| 20 | 1.5 | 3.75 | 9 |
| 30 | 1.5 | 3.75 | 14 |
| 40 | 1.5 | 3.75 | 19 |

The apparatus used in measurement of sheet deformation was ATOS Capsule 200 MV200 (Carl Zeiss Sp. z o.o., Warsaw, Poland) – Figure 8. The measurement system is ensuring the measurement parameters according to VDI/VDE 2634 Part 3 standard [55] in line with the GOM Acceptance Test. The maximum deviations after acceptance test, for used 3D scanner, are probing error form (0.001 mm), probing error (0.003 mm), sphere spacing error (0.008 mm) and length measurement error (0.009 mm). Additionally after each five measurement, to ensure high quality results, the scanner was calibrated. The references points used to generate the mesh model were placed on the measurement table and measurement grip.

 doi:10.20944/preprints202402.1272.v1



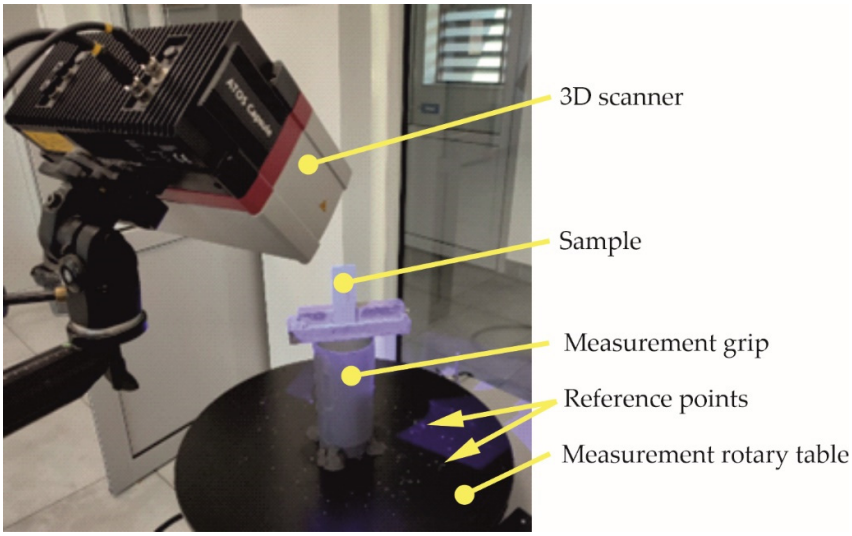


**Figure 8.** The measurement stand with 3D Atos Capsule scanner.

To generate the measurement mesh, two measurement series were made, each with 10 pictures using automatic work with a rotary table. Each of the shots consists of two photos recorded by the cameras of the measurement plate – Figure 9. The transformation of individual shots takes place through common reference points.

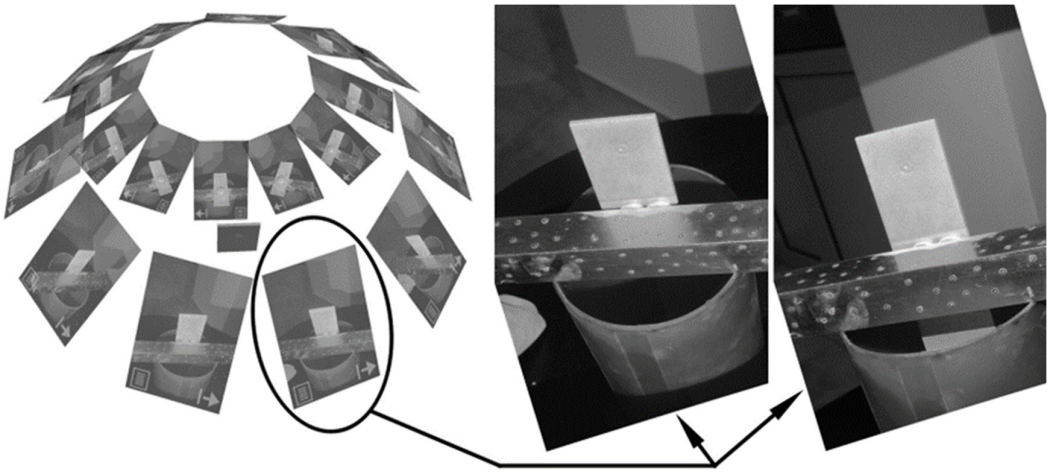

**Figure 9.** The summary of the performed measurement series, with a specification of one shot as 2 photos.

It was assumed that the sheet surface deformation comparison would be made on samples with a common coordinate system adopted in accordance with Figure 10a. The bottom of the die was taken as the main reference plane (Z=0.00). This plane was determined by the "Fitting Plane" method in GOM Inspect program. The origin for the X and Y axes was determined from the torus (as result from the cross-section of the plane parallel to the Z plane and the formed ring). The rotation of XYZ coordinate system was set as parallel to the side surface of the sheet samples – Figure 10b.

Preprints.org (www.preprints.org) | NOT PEER-REVIEWED | Posted: 22 February 2024 doi:10.20944/preprints202402.1272.v1



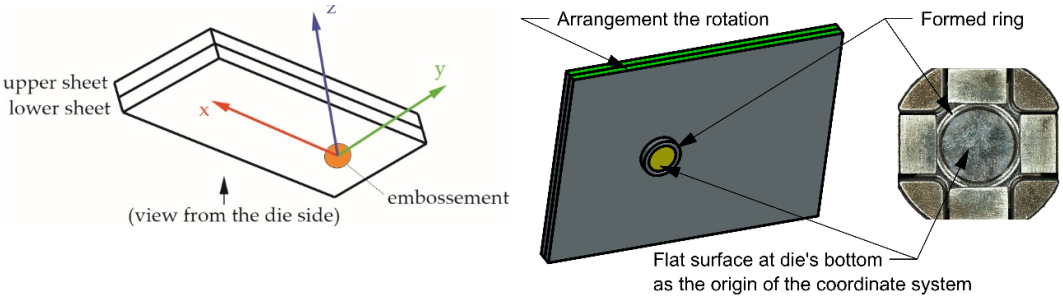


**Figure 10.** The measurement coordinate system (a) and elements used to determining and positioning axis system (b).

## 3. Results and discussions

### *3.1. Forming process of the clinch-rivet joint*

During the clinch-riveting process the forming force was measured and recorded for each joint combination seven times. For determining the mean values ($\overline{x_n}$), standard deviation ($s$) and coefficient of variation ($c_v$) five recorded values were taken into account. Calculated parameters (Equations (1)–(4)) are presented in Table 4. For each sheet thickness and width forming force-displacement diagrams are presented in Figure 11.

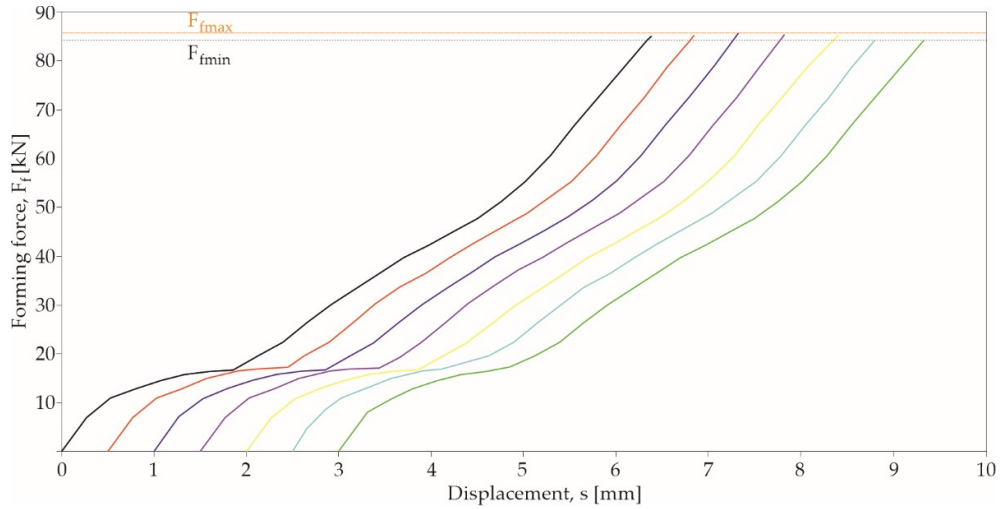


**Figure 11.** The force-displacement diagrams of clinch-riveting process for one sample combination ($b$=20 mm, $t$=1mm) – diagrams move by each other of 0.5mm.

$$\overline{x_n} = \frac{\sum_{i=1}^{n} x_i}{n} \tag{1}$$

$$s = \sqrt{\frac{1}{n-1} \cdot \sum_{i=1}^{n} (x_i - \overline{x_n})^2} \tag{2}$$

$$c_v = \frac{s}{\overline{x_n}} \cdot 100\% \tag{3}$$

 doi:10.20944/preprints202402.1272.v1



where:
$\overline{x_n}$ – mean values of forming force (kN),
$x_i$ – simple values of forming force (kN),
$n$ – number of measurements,
$s$ – standard deviation (kN),
$c_v$ – coefficient of variation (%).

$$E_f = \int_{s=0}^{s_{Fmax}} F_f \cdot ds \tag{4}$$

where:
$E_f$ – forming energy (J),
$s$ – displacement (mm),
$s_{Fmax}$ – displacement for maximum forming force (mm),
$F_f$ – forming force (kN),

 doi:10.20944/preprints202402.1272.v1



**Table 4.** Mean values of forming force and statistical parameters.

| Sample nomenclature | Sheet width *b*, [mm] | Sheet thickness *t*, [mm] | Forming force $F_f$, [kN] | Standard deviation *s*, [kN] | Coefficient of variation $c_v$, [%] | Forming energy $E_f$, [J] |
|---|---|---|---|---|---|---|
| 1-2 | 20 | 1 | 85.18 | 0.398 | 0.467 | 232 |
| 1-3 | 30 | 1 | 87.35 | 0.397 | 0.454 | 236 |
| 1-4 | 40 | 1 | 87.77 | 0.426 | 0.485 | 237 |
| 2-2 | 20 | 1.5 | 72.32 | 0.398 | 0.550 | 210 |
| 2-3 | 30 | 1.5 | 74.57 | 0.356 | 0.477 | 218 |
| 2-4 | 40 | 1.5 | 74.29 | 0.416 | 0.560 | 213 |

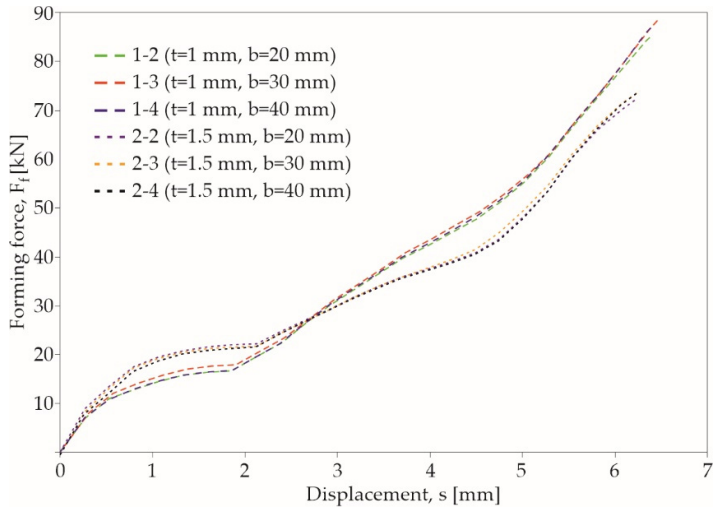


**Figure 12.** The comparison of the force-displacement diagrams of clinch-riveting process.

Changing the distance of the joint from the sheet edge from 20 mm to 10 mm caused the sheet material to flow more freely in the radial direction outside the die, which resulted in the lowering the force necessary to form the joint by 2.95% for sheets with a thickness of 1 mm, and by 2.65% for sheets with a thickness 1.5mm.

By reducing the distance of the joint from the edge of the sheet, the forming force and, consequently, the demand for forming energy can be reduced. Another way to reduce the energy absorption of the joint formation process is to use a rivet of a different hardness [30], use a tubular rivet [27], change the insertion depth of the rivet [56].

### *3.2. Sheet deformation measurement before joining process*

To ensure that there was sheet deformation before joining (for example deformation from sample cutting process), all sheet samples were scanned with ATOS Capsule scanner. Examples of sheet area scan were presented in Figure 13. Average sheet thickness and sheet width were given in Table 5. For each sheet strips the measured dimensions were on acceptable level.

 doi:10.20944/preprints202402.1272.v1



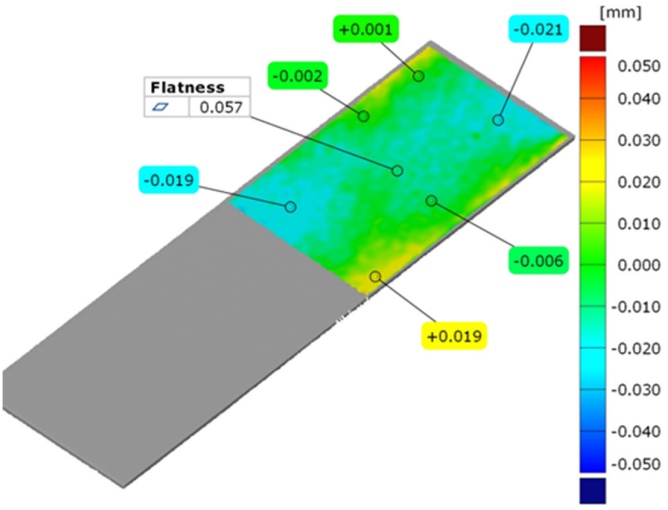


**Figure 13.** The result of the sheet deviation before joining.

**Table 5.** Values of the sheet dimensions and deviations (average values).

| Measured parameter | Values |
|---|---|
| Sheet thickness *t*, [mm] | 1 |
| Manufacturer sheet thickness tolerance, [mm] | ±0.07 |
| Measured sheet thickness, [mm] | 0.98 |
| Sheet width *b*, [mm] | 20, 30, 40 |
| Sheet width tolerance, [mm] | ±0.1 |
| Measured sheet width, [mm] | 20.07, 30.05, 40.03 |
| Sheet thickness *t*, [mm] | 1.5 |
| Manufacturer sheet thickness tolerance, [mm] | ±0.11 mm |
| Measured sheet thickness, [mm] | 1.45 |
| Sheet width *b*, [mm] | 20, 30, 40 |
| Sheet width tolerance, [mm] | ±0.1 |
| Measured sheet width, [mm] | 20.05, 30.06, 40.03 |

All samples were laser cut from the same sheet metal. Measurements of the sheet metal strips before joining showed that the actual dimensions of the samples were consistent with the dimensional parameters provided by the manufacturer.

*3.3. Sheet deformation measurement after joining process*

Based on the permanent elements of the die - the flat surface of the die bottom, the groove on the die bottom and the side surface of the sheets, coordinate systems were created for all joints. The surface and torus fitting parameters are presented in Table 6.

**Table 6.** The results of geometry fitting used for the determining of the axis system.

| Adjustment result | | Sheet dimension *b* x *t*, [mm x mm] | | | | | |
|---|---|---|---|---|---|---|---|
| | | 20x1 | 30x1 | 40x1 | 20x1.5 | 30x1.5 | 40x1.5 |
| Fitting plane (axis Z=0.0 mm) | Minimum mm | -0.031 | -0.004 | -0.005 | -0.0036 | -0.0045 | -0.0049 |
| | Maximum mm | 0.0045 | 0.0068 | 0.0073 | 0.0041 | 0.0058 | 0.0046 |
| | Sigma mm | 0.002 | 0.0029 | 0.0036 | 0.0022 | 0.0029 | 0.0028 |
| | Residual mm | 0.0017 | 0.0024 | 0.0031 | 0.0019 | 0.0024 | 0.0025 |

 doi:10.20944/preprints202402.1272.v1



| | | | | | | | |
|---|---|---|---|---|---|---|---|
| | Number of nodes for base creation | 608 | 691 | 904 | 521 | 568 | 631 |
| Fitting torus (axes X=0.0. Y=0.0 mm) | Minimum mm | -0.0187 | -0.0219 | -0.0142 | -0.0196 | -0.0297 | -0.0187 |
| | Maximum mm | 0.0197 | 0.0216 | 0.0103 | 0.0128 | 0.0148 | 0.0139 |
| | Sigma mm | 0.0069 | 0.074 | 0.0049 | 0.0062 | 0.0086 | 0.0068 |
| | Residual mm | 0.0054 | 0.0057 | 0.0039 | 0.0049 | 0.0065 | 0.0053 |

In the area close to the rivet the measurement system didn't ensure appropriate values. For the position of the punch system at the level of the upper surface of the sheet, as recommended by TOX manufacturer, the joints made of 1 mm sheet thickness at the point contact with the punch had a larger size. This was due to the greater pressing of the rivet – the distance between die and punch was smaller than for 1.5 mm sheet thicknesses. In addition, the Rmin value of 3.75 mm was selected to eliminate defects on the mesh after the process of polygonization of measurement data, presented in Figure 14 below as sub-points 1 to 3 (places where light reflections occurred resulting in the lack of the scanned area or representation deviating from reality) in connection with adopted measurement method.

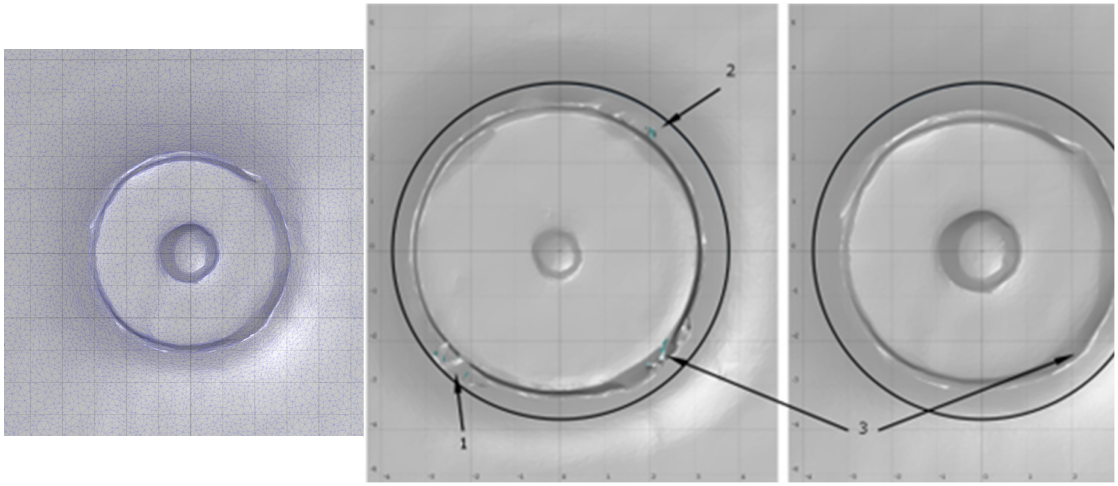


(a) (b)

**Figure 14.** Sample of the mesh grid (a) and the measurement mesh defects close to the punch-sheet contact area (b).

For determine the sheet deformation, after clinch riveting process, all joint were scanned by using ATOS scanner. Deformation of lower and upper sheet in the area of joint were analyzed on the base of 3d model obtained from measurement. The part of the samples in the equipment grip area was didn't take into account for results analyzing. In Figure 15 the views of 3D model from lower and upper sheet were presented.

 doi:10.20944/preprints202402.1272.v1



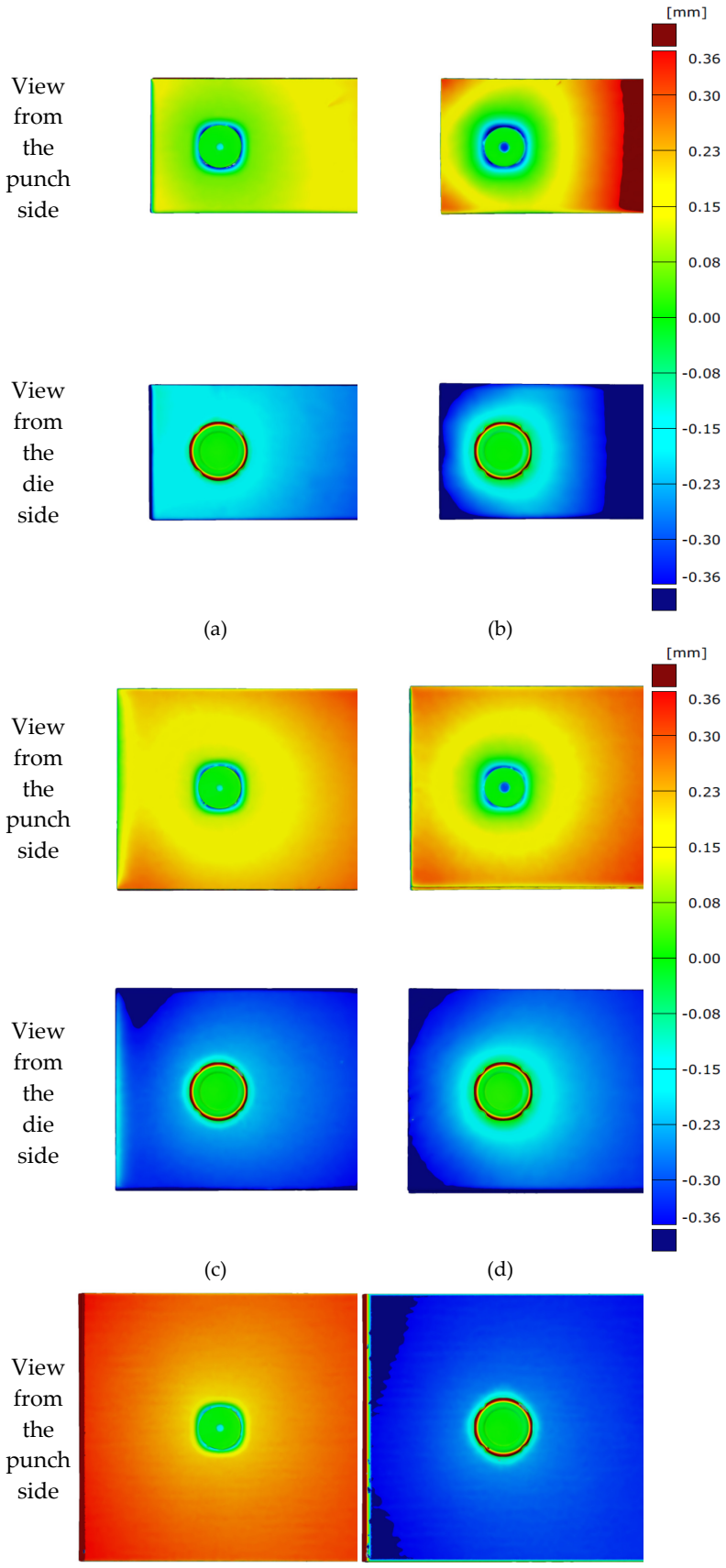

Preprints.org (www.preprints.org) | NOT PEER-REVIEWED | Posted: 22 February 2024 doi:10.20944/preprints202402.1272.v1



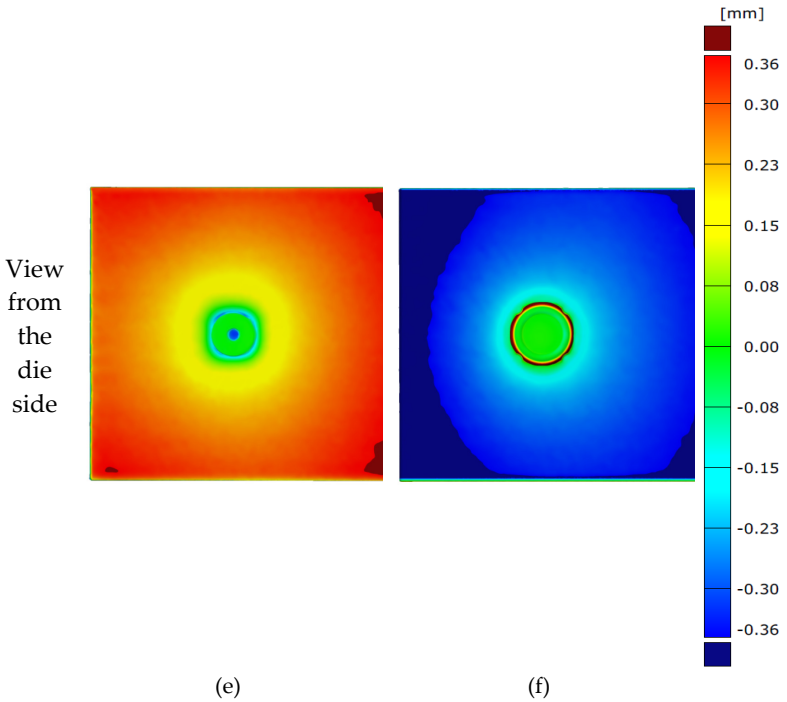


**Figure 15.** Samples of the sheets deformations with clinch-rivet joints for sheet width *b* and thickness *t*: a) 20x1 mm, b) 20x1.5 mm, c) 30x1 mm, d) 30x1.5 mm, e) 40x1 mm, f) 40x1.5 mm.

For each samples the shape of the deformation, in the area close to the rivet, reproduces the shape of the die with movable segments. For fixed segments of the die, from rivet side close to the rivet, the sheet deformation along the measurement angle $\alpha$ equal 45°, 135°, 225° and 315° was bigger than for angles 0°, 90°, 180° and 270°. The movement of die sliding element caused that the more sheet material can flow in the space between fixed part of the die and movable segments. Hence the sheet deformation in this places is smaller than for die fixed element – sheet material is less compressed. Deformations of the sheet, with the increase of the distance between rivet axis and measuring point, were changing to circular shape. By increasing the sheet width the area of upper and lower sheet deformation lower than ±0.1 mm significantly decrease. The material close to the sheet edges, for 40 mm sheet width, didn't allow to change the sheet dimensions.

For the sheets thickness 1.5 mm and width 20 mm the bulk (rivet pressed in the sheets caused the sheet material flow) of the sheet appear along the 180° angle - Figure 16b. For lower sheet dimension between rivet axis and sheet edge (angle 180°) increase of 0.11 mm and upper sheet increase of 0.09 mm – the linearity deviation. The sheet width at the sheet corners was also changed form 20 mm to 20.34 for lower sheet and 20.19 for upper sheet. For the 90° and 270° angles the sheet material was partially blocked by sheet material along to the measurement grip area – the sample was changes to 20.34 for lower sheet and 20.19 for upper sheet. The material of the sheet along the 0° angle didn't allow to push outside the sheet material. For other sheet width (30, 40 mm) and the sheet thickness 1.5 mm and for all samples of 1.00 mm the change of width observed was on the 0.03 mm. The linearity deviation of the sheet was presented in Table 7. For the sheet thickness 1.0 mm and 1.5 mm and width 40 mm the measured deformations were presented in Table 8. The measurement points coordinates for 3D models for all joints were presented in Figure 7. The origin point of the axis system was always in the center point of the die bottom. The linearity deviations for other sheet width and thickness was at similar level – about 0.02 mm. So the sheet dimension after joining process significantly change only for sheet thickens 20 mm and thickness of 1.0 mm.

 doi:10.20944/preprints202402.1272.v1



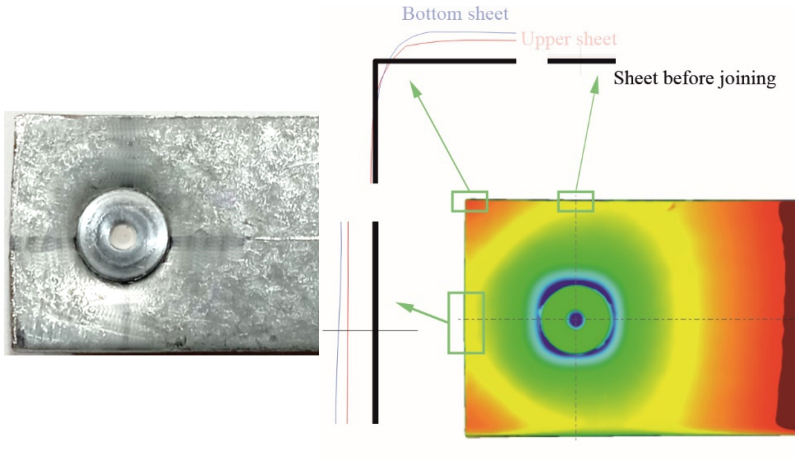


(a) (b)

**Figure 16.** Example of sheet deformation in a clinch-rivet joint (sheet thickness *t*=1.5 mm, sheet width *b*=20 mm): a) real view from the die side, b) view form punch side of the joint CAD model.

**Table 7.** The sheet linearity deviation after clinch-riveting process.

| **Sample nomenclature** | 1-2 | 1-3 | 1-4 | 2-2 | 2-3 | 2-4 |
|---|---|---|---|---|---|---|
| **Sheet thickness *t*, [mm]** | 1 | 1 | 1 | 1.5 | 1.5 | 1.5 |
| **Sheet width *b*, [mm]** | 20 | 30 | 40 | 20 | 30 | 40 |
| **Lower sheet dimension for angle 90° and 270°** | 0.29 | 0.04 | 0.02 | 0.03 | 0.01 | 0.01 |
| **Upper sheet dimension for angle 90° and 270°** | 0.14 | 0.03 | 0.01 | 0.01 | 0.02 | 0.01 |
| **Lower sheet dimension for angle 180°** | 0.11 | 0.03 | 0.03 | 0.02 | 0.01 | 0.01 |
| **Upper sheet dimension for angle 180°** | 0.09 | 0.02 | 0.03 | 0.02 | 0.01 | 0.01 |
| **Average sheet width before joining, [mm]** | 20.07 | 30.05 | 40.03 | 20.05 | 30.06 | 40.03 |

**Table 8.** Measured of profile point deviation for clinch-riveted joint made for 40 mm width sheets.

| Sheet thickness *t*, [mm] | 1 | 1 | 1 | 1 | 1 | 1 | 1.5 | 1.5 | 1.5 | 1.5 | 1.5 | 1.5 |
|---|---|---|---|---|---|---|---|---|---|---|---|---|
| Measurement angle $\alpha$, [°] | 0° | 45° | 90° | 180° | 225° | 270° | 0° | 45° | 90° | 180° | 225° | 270° |
| Values of the point deviations | | | | | | | | | | | | |
| Measurement radius *R*, [mm] | | | | | | | | | | | | |
| 3.75 | 0.08 | -0.03 | 0.03 | 0.06 | -0.05 | 0.07 | 0.02 | -0.07 | -0.02 | 0.01 | -0.06 | 0.02 |
| 4.00 | 0.14 | 0.05 | 0.10 | 0.13 | 0.05 | 0.14 | 0.05 | -0.01 | 0.02 | 0.05 | -0.01 | 0.05 |
| 4.25 | 0.17 | 0.11 | 0.14 | 0.17 | 0.11 | 0.18 | 0.08 | 0.02 | 0.05 | 0.07 | 0.03 | 0.08 |
| 4.50 | 0.19 | 0.15 | 0.17 | 0.19 | 0.15 | 0.2 | 0.10 | 0.05 | 0.07 | 0.09 | 0.05 | 0.10 |
| 4.75 | 0.20 | 0.17 | 0.19 | 0.20 | 0.18 | 0.21 | 0.11 | 0.08 | 0.09 | 0.10 | 0.07 | 0.11 |
| 5.00 | 0.21 | 0.19 | 0.20 | 0.20 | 0.20 | 0.22 | 0.13 | 0.09 | 0.10 | 0.11 | 0.09 | 0.13 |
| 5.25 | 0.21 | 0.19 | 0.20 | 0.21 | 0.21 | 0.22 | 0.13 | 0.11 | 0.11 | 0.12 | 0.1 | 0.14 |
| 5.50 | 0.21 | 0.20 | 0.20 | 0.21 | 0.21 | 0.22 | 0.14 | 0.12 | 0.12 | 0.13 | 0.12 | 0.14 |

 doi:10.20944/preprints202402.1272.v1



| | | | | | | | | | | | | |
|---|---|---|---|---|---|---|---|---|---|---|---|---|
| 5.75 | 0.21 | 0.20 | 0.20 | 0.21 | 0.22 | 0.22 | 0.15 | 0.13 | 0.13 | 0.13 | 0.13 | 0.15 |
| 6.00 | 0.21 | 0.20 | 0.20 | 0.22 | 0.22 | 0.22 | 0.15 | 0.14 | 0.14 | 0.14 | 0.13 | 0.15 |
| 7.00 | 0.22 | 0.21 | 0.21 | 0.22 | 0.22 | 0.23 | 0.17 | 0.16 | 0.16 | 0.16 | 0.16 | 0.17 |
| 8.00 | 0.23 | 0.22 | 0.22 | 0.23 | 0.24 | 0.24 | 0.19 | 0.18 | 0.18 | 0.18 | 0.18 | 0.19 |
| 9.00 | 0.24 | 0.23 | 0.23 | 0.24 | 0.24 | 0.24 | 0.21 | 0.20 | 0.19 | 0.20 | 0.20 | 0.20 |
| 10.00 | 0.24 | 0.23 | 0.24 | 0.25 | 0.25 | 0.25 | 0.22 | 0.22 | 0.21 | 0.21 | 0.22 | 0.22 |
| 11.00 | 0.25 | 0.24 | 0.24 | 0.26 | 0.26 | 0.26 | 0.23 | 0.22 | 0.22 | 0.22 | 0.23 | 0.23 |
| 12.00 | 0.25 | 0.24 | 0.25 | 0.27 | 0.27 | 0.26 | 0.24 | 0.24 | 0.24 | 0.23 | 0.24 | 0.24 |
| 13.00 | 0.26 | 0.25 | 0.25 | 0.27 | 0.27 | 0.27 | 0.26 | 0.25 | 0.25 | 0.24 | 0.26 | 0.25 |
| 14.00 | 0.27 | 0.26 | 0.26 | 0.28 | 0.28 | 0.27 | 0.27 | 0.26 | 0.26 | 0.25 | 0.26 | 0.26 |
| 15.00 | 0.27 | 0.26 | 0.26 | 0.29 | 0.29 | 0.27 | 0.28 | 0.27 | 0.27 | 0.26 | 0.27 | 0.27 |
| 16.00 | 0.27 | 0.27 | 0.27 | 0.3 | 0.29 | 0.28 | 0.29 | 0.28 | 0.28 | 0.27 | 0.29 | 0.28 |
| 17.00 | 0.28 | 0.27 | 0.27 | 0.3 | 0.3 | 0.28 | 0.3 | 0.29 | 0.29 | 0.28 | 0.29 | 0.29 |
| 18.00 | 0.29 | 0.28 | 0.27 | 0.31 | 0.3 | 0.29 | 0.31 | 0.3 | 0.3 | 0.28 | 0.3 | 0.3 |
| 19.00 | 0.29 | 0.28 | 0.28 | 0.32 | 0.31 | 0.29 | 0.32 | 0.31 | 0.31 | 0.26 | 0.31 | 0.3 |

For all joint, based on the 3d models, the sheet profile after clinch-riveting joining process were determined along the angles $\alpha$=0°, 45°, 90°, 180°, 225° and 270° – Figure 17.

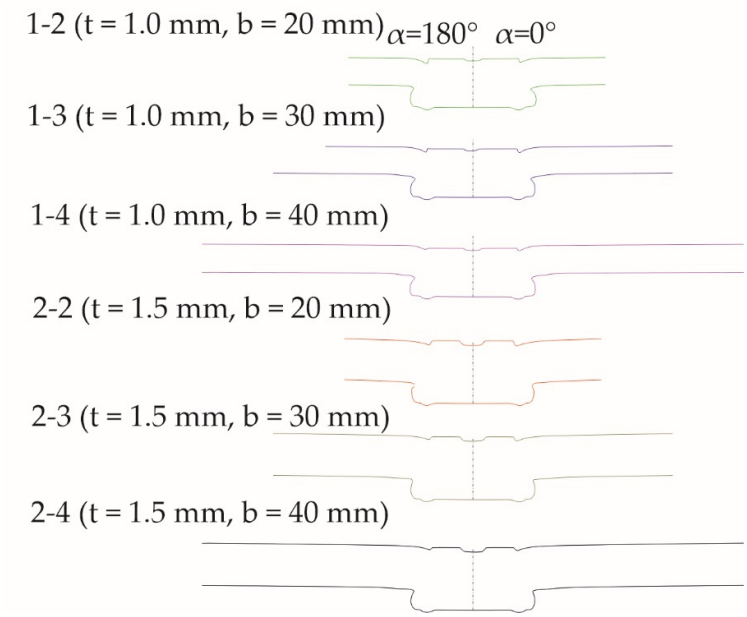


(a)

 doi:10.20944/preprints202402.1272.v1



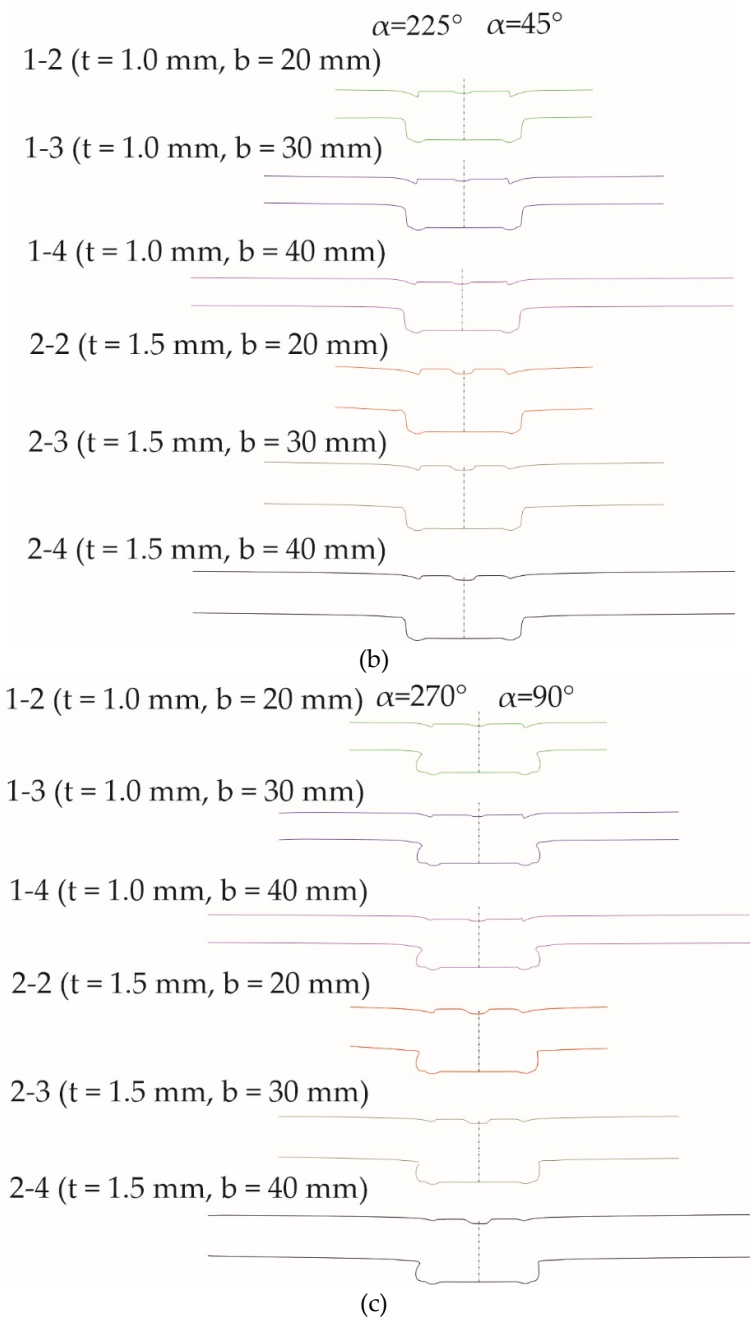


**Figure 17.** Profiles of the sheets: a) $\alpha$=0° and $\alpha$=180°, b) $\alpha$=45° and $\alpha$=225°, c) $\alpha$=90° and $\alpha$=270°.

For a sheets width of 20 mm (Figure 18 – red line) and a thickness of 1.5, it can be seen that the deformation of the upper and lower sheets in the area of the rivet is greater than for the widths of 30 mm (Figure 18 – green line) and 40 mm (Figure 18 – black line). The smaller amount of material around the joint causes the sheet to deform more freely than in the case of wider sheet samples.

 doi:10.20944/preprints202402.1272.v1



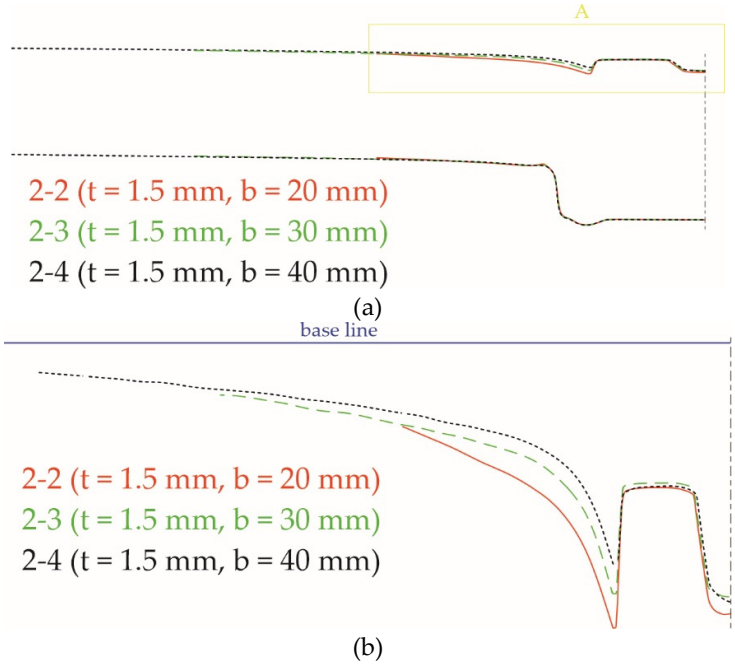


**Figure 17.** Profiles of the sheet with 1.5 mm thickness ($\alpha$=45°): a) half of the cross-section, b) 10x zoom in y axis of A area.

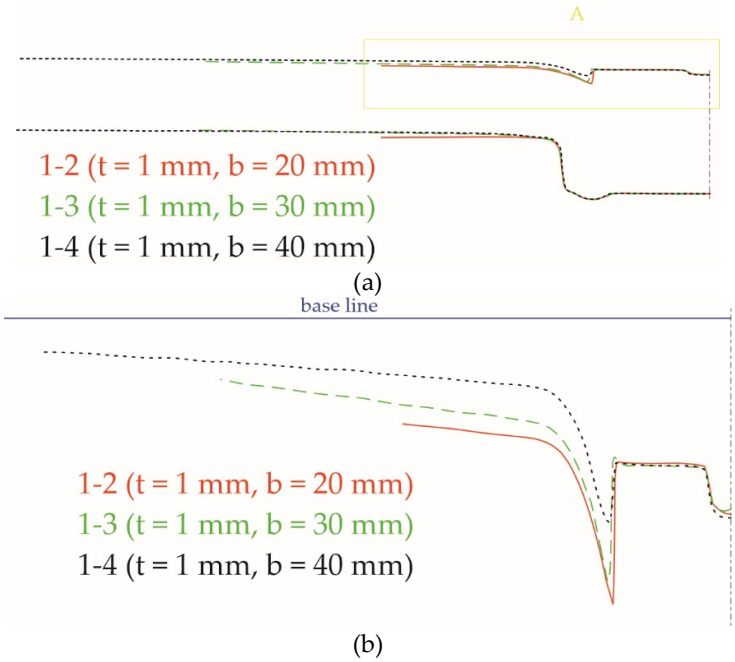


**Figure 18.** Profiles of the sheet with 1.0 mm thickness ($\alpha$ =45°): a) half of the cross-section, b) 10x zoom in y axis of A area.

For sheets with a thickness of 1 mm, the blank holder causes that for smaller widths, the sheet material around it is pressed deeper – Figure 18.

Changing the thickness of the joined sheets from 1.0 mm (Figure 19 – red line) to 1.5 mm (Figure 19 – green line) with the same geometry of the forming die and the rivet causes that more material fills the same space in the die, which causes greater deformations in the joint area. For the angle $\alpha$=225° the deformation in higher due to less stiffness of the sheet than for angle $\alpha$=45°.

 doi:10.20944/preprints202402.1272.v1



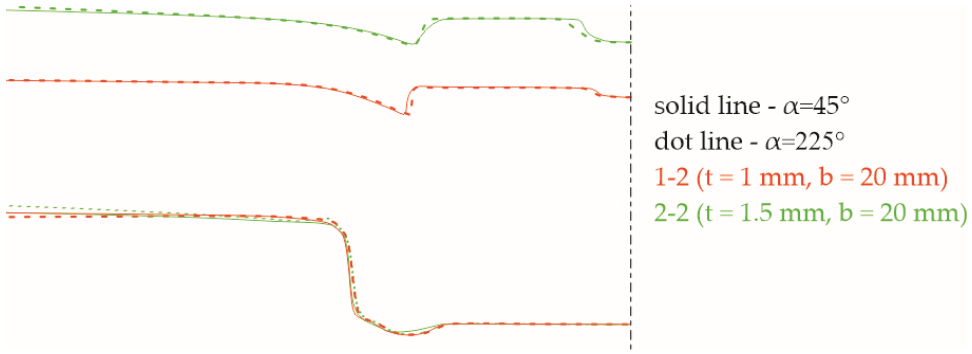


**Figure 19.** Profiles of the sheet with 20 mm width and angle $\alpha$=45° and $\alpha$=225° (sheet thickness 1.5 mm - green line and 1 mm - red line).

The range and size of sheet deformation for the angle $\alpha$=0° and $\alpha$ =180° is almost identical for all tested variants. Slight differences are visible for the width of 20 mm and the thickness of 1.5mm. For all angles the course of sheet deformation were the same. There were slight differences in values of deformation caused by the sheet material flow during the joint formation. In Figure 20 the joint profile in the die groove (green line) and profile in the space of movable segments (red line) were compared.

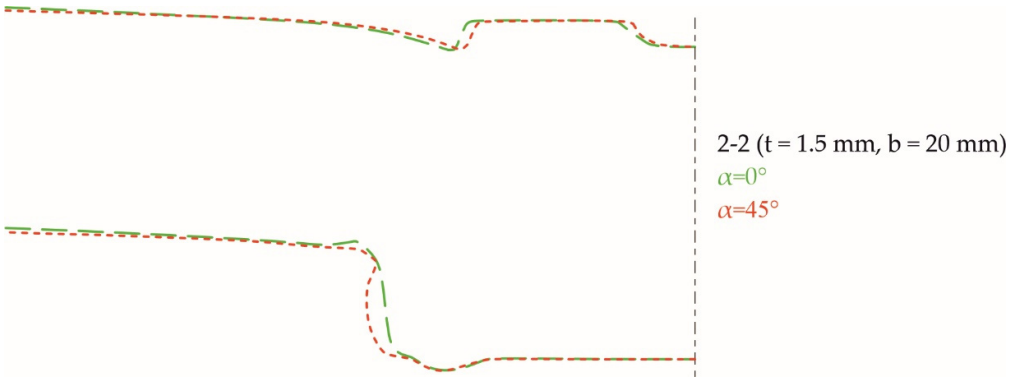


**Figure 20.** Profiles of the sheet with 20 mm width ($\alpha$=0° - green line and $\alpha$=45° - red line).

## 4. Conclusions

In this paper the analysis of the DX51D steel sheet deformation after clinch-riveting process was presented. For two different sheet thickness (1.0 mm and 1.5 mm), three sheet width (20, 30 and 40 mm) the forming forces and deformation of sheets were measured. The influence of the angle, between die movable segments and sheet contours, on the profile shape was done. The conducted research and results led to conclusions. The most important conclusions are:

- The energy consumption of the forming force and the forming process can be reduced by reducing the distance between the joint axis and the edge of the sheet. Forming force was reduced by 2.95% for sheets with a thickness of 1 mm and by 2.65% for sheets with a thickness 1.5 mm when the distance between the joint axis and the edge of the sheet was reduced from 20 mm to 10 mm.
- The deformation of the sheet depends on the angle between the movable segments and the edge of the sheet. For angles $\alpha$=0° and $\alpha$=180° there were no differences in sheet deformation despite that for 180° there was less material to the sheet edge than for 0°.
- The differences in the sheet deformation for angles $\alpha$=45° and $\alpha$=225° are caused by the lower stiffness of the sheet from the closer edge ($\alpha$=225°).
- For a small distance between the joint axis and the edge of the sheet, the bulk can be obtained. For sheet width 20 mm and thicknesses 1 mm and 1.5 mm, the material of sheet was pushed

more intensively in the radial directions for all angles without 0° - sheet material along 0° blocked sheet deformation in that direction.

**Author Contributions:** Conceptualization, W.W., Ł.B. and J.M.; methodology, W.W., J.M. and Ł.B.; software, W.W.; validation, W.W. and Ł.B.; formal analysis, W.W. and J.M.; investigation, Ł.B., J.M. and W.W.; resources, J.M.; data curation, Ł.B.; writing—original draft preparation, W.W.; writing—review and editing, J.M. and Ł.B.; visualization, W.W., Ł.B. and J.M.; supervision, J.M.; project administration, W.W.; funding acquisition, Ł.B., J.M. and W.W. All authors have read and agreed to the published version of the manuscript.

**Funding:** This research received no external funding.

**Institutional Review Board Statement:** Not applicable.

**Informed Consent Statement:** Not applicable.

**Data Availability Statement:** Data available on request due to restrictions.

**Conflicts of Interest:** The authors declare no conflicts of interest.

## References

1. Leite, W. O.; Campos Rubio, J. C.; Mata, F.; Hanafi, I.; Carrasco, A. Dimensional and Geometrical Errors in Vacuum Thermoforming Products: An Approach to Modeling and Optimization by Multiple Response Optimization. Meas. Sci. Rev. 2018, 3, 113-122.
2. Valíček, J.; Harničárová, M.; Kušnerová, M.; Zavadil, J.; Grznárik, R. Method of Maintaining the Required Values of Surface Roughness and Prediction of Technological Conditions for Cold Sheet Rolling. Meas. Sci. Rev. 2014, 3, 144-151.
3. Hultman, H.; Cedergren, S.; Wärmefjord, K.; Söderberg, R. Predicting Geometrical Variation in Fabricated Assemblies Using a Digital Twin Approach Including a Novel Non-NominalWelding Simulation. Aerospace, 2022, 9, 512.
4. Meschut, G.; Janzen, V.; Olfermann, T. Innovative and Highly Productive Joining Technologies for Multi-Material Lightweight Car Body Structures. J. Mater. Eng. Perform. 2014, 23, 1515-1523.
5. Eckert, A.; Israel, M.; Neugebauer, R.; Rössinger, M.; Wahl, M.; Schulz, F. Local–global approach using experimental and/or simulated data to predict distortion caused by mechanical joining technologies. Prod. Eng. Res. Devel. 2013, 7, 339-349.
6. Varis, J.P.; Lepisto, J. A simple testing-based procedure and simulation of the clinching process using finite element analysis for establishing clinching parameters. Thin. Wall. Struct. 2003, 41, 691-709.
7. Zheng, B.; Yu, H.; Lai, X. Assembly deformation prediction of riveted panels by using equivalent mechanical model of riveting process. Int. J. Adv. Manuf. Technol. 2017, 92, 1955-1966.
8. He, X.; Wang, Y.; Lu, Y. et al. Self-piercing riveting of similar and dissimilar titanium sheet materials. Int. J. Adv. Manuf. Technol. 2015, 80, 2105-2115.
9. Xing, B.; He, X.; Zeng, K. et al. Mechanical properties of self-piercing riveted joints in aluminum alloy 5052. Int. J. Adv. Manuf. Technol. 2014, 75, 351-361.
10. Zhang, X.; He, X.; Gu, F.; Ball, A. Self-piercing riveting of aluminium–lithium alloy sheet materials. J. Mater. Process. Technol. 2019, 268, 192-200.
11. Zhao, L.; He, X.; Xing, B.; Zhang, X.; Cheng, Q.; Gu, F.; Ball, A. Fretting behavior of self-piercing riveted joints in titanium sheet materials. J. Mater. Process. Technol. 2017, 249, 246-254.
12. Mucha, J.; Kaščák, L.; Spišák, E. Joining the car-body sheets using clinching process with various thickness and mechanical property arrangements. Arch. Civ. Mech. Eng. 2011, 1, 135-148.
13. Lee, C.-J.; Shen, G.; Kim, B.-M.; Lambiase, F.; Ko, D.-C. Analysis of failure-mode dependent joint strength in hole clinching from the aspects of geometrical interlocking parameters. Metals, 2018, 8, 1020.
14. Zhang, Y.; He, X.; Wang, Y. et al. Study on failure mechanism of mechanical clinching in aluminium sheet materials, Int. J. Adv. Manuf. Technol. 2018, 96, 3057-3068.
15. Abe, Y.; Kato, T.; Mori, K-I.; Nishino, S. Mechanical clinching of ultra-high strength steel sheets and strength of joints. J. Mater. Process. Technol. 2014, 10, 2112-2118.
16. Ge, Y.; Xia, Y. Mechanical characterization of a steel-aluminum clinched joint under impact loading. Thin. Wall. Struct. 2020, 151, 106759.
17. Lee, C.-J.; Shen, G.; Kim, B.-M.; Lambiase, F.; Ko, D.-C. Analysis of failure-mode dependent joint strength in hole clinching from the aspects of geometrical interlocking parameters. Metals, 2018, 8, 1020.
18. Grimm, T.; Drossel, W.-G. Process development for self-pierce riveting with solid formable rivet of boron steel in multi-material design. Procedia Manuf. 2019, 29, 271-279.
19. Neugebauer, R.; Rössinger, M.; Wahl, M.; Schulz, F.; Eckert, A.; Schützle, W. Predicting Dimensional Accuracy of Mechanically Joined Car Body Assemblies. Key Eng. Mater. 2011, 473, 973-980.

 doi:10.20944/preprints202402.1272.v1




20. Neugebauer, R.; Jesche, F.; Kraus, C.; Hensel, S. Mechanical joining with self piercing solid-rivets at elevated tool velocities. The 14th International ESAFORM Conference on Material Forming: ESAFORM 2011. AIP Conference Proceedings, 2011, 1353, 1278-1283.
21. Mucha, J. The effect of material properties and joining process parameters on behavior of self-pierce riveting joints made with the solid rivet. Mater. Des. 2013, 52, 932-946.
22. Mucha, J. The numerical analysis of the effect of the joining process parameters on self-piercing riveting using the solid rivet. Arch. Civil Mech. Eng. 2014, 14, 444-454.
23. Mucha, J. The failure mechanics analysis of the solid self-piercing riveting joints. Eng. Fail. Anal. 2015, 47, 77-88.
24. Neugebauer, R.; Jesche F.; Israel, M. Enlargement of the application range of solid punch riveting by two-piece dies. Int. J. Mater. Form. 2010, 3, 999-1002.
25. Mucha, J.; Kaščák L'.; Spišák, E. The experimental analysis of forming and strength of clinch riveting sheet metal joint made of different materials. Adv. Mech. Eng. 2013, 5.
26. Mucha, J.; Kaščák, Ľ.; Witkowski, W. Research on the influence of the AW 5754 aluminum alloy state condition and sheet arrangements with AW 6082 aluminum alloy on the forming process and strength of the clinch-rivet joints. Materials, 2021, 14, 2980.
27. Mucha, J.; Boda, Ł.; Witkowski, W. Geometrical parameters and strength of clinching joint formed with the use of an additional rivet. Arch. Civ. Mech. Eng. 2023, 114, 1-16.
28. Ren, X.; Chen, C.; Ran, X.; Gao, X.; Gao, Y. Investigation on lightweight performance of tubular rivet-reinforced joints for joining AA5052 sheets. J. Braz. Soc. Mech. Sci. Eng. 2021, 43, 333.
29. Chen, C.; Wu, J.; Li, H. Optimization design of cylindrical rivet in flat bottom riveting. Thin. Wall. Struct. 2021, 168, 108292.
30. Mucha, J.; Boda, Ł.; Witkowski, W.; Poręba, M. Mixed-mode loading tests for determining the mechanical properties of clinched joints with an additional rivet used in the assembly of thin-walled structures. Thin. Wall. Struct. 2023, 190, 110965.
31. Chen, C.; Zhang, X.; Wen, C.; Yin, Y. Effect of blank holder force on joining quality of the flat clinch-rivet process. Int. J. Adv. Manuf. Technol. 2022, 121, 6315-6323.
32. Abe, Y.; Maeda, T.; Yoshioka, D.; Mori, K.-I. Mechanical clinching and self-pierce riveting of thin three sheets of 5000 series aluminium alloy and 980 MPa grade cold rolled ultra-high strength steel. Materials, 2020, 13, 4741.
33. Mori, K.; Abe, Y.; Kato, T.; Sakai, S. Self-pierce riveting of three aluminium alloy and mild steel sheets. In AIP Conference Proceedings; AIP Publishing: College Park, MD, USA, 2010, 1252, 673-680.
34. Abe, Y.; Kato, T.; Mori, K. Self-pierce riveting of three high strength steel and aluminium alloy sheets. Int. J. Mater. Form. 2008, 1,1271-1274.
35. Kaščák, Ľ.; Spišák, E.; Majerníková, J. Joining three car body steel sheets by clinching method. Open Eng. 2016; 6, 566-573.
36. Kaščák, L.; Spišák E.; Kubik, R.; Mucha, J. FEM analysis of clinching tool load in a joint of dual-phase steels. Strength Mater. 2016, 48, 533-539.
37. Md Abdul Karim, Siva Prasad Murugan, KiMan Bae, Jongjin Baek, Changwook Ji, Wooram Noh, Han-Ju Lee, Will Jang, Duck Bong Kim, Yeong-Do Park. Effect of top sheet materials on joint performance of self-piercing riveting. J. Weld. Join. 2022, 6, 512-524.
38. Wang, J.; Zhang, G.; Zheng, X.; Li, J.; Li, X.; Zhu, W.; Yanagimoto, J. A self-piercing riveting method for joining of continuous carbon fiber reinforced composite and aluminum alloy sheets. Compos. Struct. 2021, 259, 113219.
39. Sankaranarayanan, R.; Hynes, N.; Nikolova, M. P.; Królczyk, J. B. Self-pierce riveting: Development and assessment for joining polymer—Metal hybrid structures in lightweight automotive applications. Polymers, 2023, 15, 4053.
40. Jäckel, M.; Grimm, T.; Niegsch, R.; Drossel, W.-G. Overview of current challenges in self-pierce riveting of lightweight materials. Proceedings, 2018, 2, 384.
41. Gröger, B.; Troschitz, J.; Vorderbrüggen, J.; Vogel, Ch.; Kupfer, R.; Meschut, G.; Gude, M. Clinching of thermoplastic composites and metals—A comparison of three novel joining technologies. Materials, 2021, 9, 2286.
42. Galińska, A.; Galiński, C. Mechanical Joining of Fibre Reinforced Polymer Composites to Metals—A Review. Part II: Riveting, Clinching, Non-adhesive form-locked joints, pin and loop joining. Polymers, 2020, 8, 1681.
43. Lambiase, F.; Scipioni, S. I.; Lee, Ch-J.; Ko, D-Ch.; Liu, F. A state-of-the-Art review on advanced joining processes for metal-Composite and metal-Polymer hybrid structures. Materials, 2021, 8, 1890.
44. Lambiase, F.; Mechanical behaviour of polymer–metal hybrid joints produced by clinching using different tools. Mater. Des. 2015, 87, 606-618.
45. Lambiase, F.; Durante, M. Mechanical behavior of punched holes produced on thin glass fiber reinforced plastic laminates. Compos. Struct. 2017, 173, 25-34.

 doi:10.20944/preprints202402.1272.v1




46. Meschut, G,; Gude, M,; Augenthaler, F,; Geske, V. Evaluation of damage to carbon- fibre composites induced by self-pierce riveting. Procedia CIRP, 2014, 18, 186-91.
47. Lambiase, F.; Paoletti, A. Friction-assisted clinching of aluminum and CFRP sheets. J. Manuf. Process. 2018, 31, 812-822.
48. Vorderbrüggen, J,; Köhler, D.; Grüber, B.; Troschitz, J.; Gude, M.; Meschut, G. Development of a rivet geometry for solid self-piercing riveting of thermally loaded CFRP-metal joints in automotive construction. Compos. Struct. 2022, 291, 115583.
49. Wiesenmayer, S.; Graser, M,; Merklein, M. Influence of the properties of the joining partners on the load-bearing capacity of shear-clinched joints. J. Mater. Process. Technol. 2020, 283, 116696.
50. Wiesenmayer, S.; Merklein, M. Potential of shear-clinching technology for joining of three sheets. J. Adv. Join. Process. 2021, 3, 100043.
51. Latorre, N.; Casellas, D.; Costa, J. A mechanical interlocking joint between sheet metal and carbon fibre reinforced polymers through punching. In 42nd Conference of the International Deep Drawing Research Group (IDDRG 2023). IOP Conf. Series: Materials Science and Engineering, 2023, 1284, 012001.
52. Lin, P-Ch.; Fang J.-Ch.; Lin, J.-W.; Tran, X. V.; Ching, Y.-Ch. Preheated (Heat-Assisted) Clinching Process for Al/CFRP Cross-Tension Specimens. Materials, 2020, 13, 4170.
53. *EN 10327:2004*; Continuously hot-dip coated strip and sheet of low carbon steels for cold forming. Technical delivery conditions. CEN: rue de Stassart 36, B-1050 Brussels, 2004.
54. *ISO 6507-1:2018*; Metallic Materials—Vickers Hardness test—Part 1: Test Method. Technical Committee ISO/TC 164, Mechanical Testing of Metals, Subcommittee SC 3, Hardness Testing. ISO: Geneva, Switzerland, 2018.
55. *VDI/VDE 2634-3:2008-12*; Optical 3D-Measuring Systems—Multiple View Systems Based on Area Scanning; Beuth Verlag GmbH: Berlin, Germany, 2008.
56. Boda, Ł.; Mucha, J.; Witkowski, W. Performance Tests of HX340 Microalloyed Steel Sheets Joined Using Clinch-Rivet Technology. Materials **2024**, 17, 596. https://doi.org/10.3390/ma17030596